THE ASTROPHYSICAL JOURNAL, 536:255–265, 2000 June 10

THE STRUCTURE OF THE VIRGO CLUSTER FROM SURFACE BRIGHTNESS FLUCTUATIONS IN *HUBBLE SPACE TELESCOPE* IMAGES

ERIC H. NEILSEN, JR., AND ZLATAN I. TSVETANOV
Department of Physics and Astronomy, Johns Hopkins University, Baltimore, MD 21218; neilsen@pha.jhu.edu
Received 1999 August 30; accepted 2000 January 12

ABSTRACT

Surface brightness fluctuations (SBF) in *Hubble Space Telescope* (*HST*) Wide Field Planetary Camera 2 images of elliptical galaxies provide the precision necessary to examine the internal structure of the Virgo galaxy cluster. In a sample of 15 elliptical galaxies with observations from the *HST* archive, we find that most galaxies are within 2 Mpc of NGC 4486, but several galaxies (including NGC 4406) are significantly in the foreground or background. The measured redshifts and distances suggest that all sample galaxies are gravitationally bound to the galaxy cluster. The SBF distances presented here show good agreement with other SBF distance measurements and with distance measurements made using other methods. We include a brief overview of the SBF method, as well as a more detailed description of the SBF calibration used with the data included in this study, which was taken in the *HST* F814W filter.

Subject headings: galaxies: clusters: individual (Virgo) — galaxies: distances and redshifts

1. INTRODUCTION

Studies of the Virgo Cluster of galaxies, including those of its X-ray gas, projected spatial distribution of members, and heliocentric velocity distribution of members indicate a complex structure of moving subclusters (or clouds) and provide a basic understanding of their nature. However, a number of questions are difficult to answer with this information alone: can the interaction between clouds account for the unusual peculiar velocities of some members? Are most members of the cluster gravitationally bound to it? Given that the X-ray cloud surrounding NGC 4406 has a projected position very close to the X-ray cloud around NGC 4486, which galaxies are associated with which X-ray clouds? Distances to member galaxies, measured to a precision comparable to the distances between the clouds or better, can help answer these questions.

One of the few distance measurement methods practically capable of such precision is the use of the magnitude of the surface brightness fluctuations (SBF) as a standard candle, a method pioneered by Tonry & Schneider (1988). In a galaxy with a smooth morphology, the stars that make up the galaxy are distributed randomly according to a smooth probability density determined by the morphology. The finite number of stars that make up the galaxy introduce a statistical fluctuation in the number of stars projected into each pixel in an image. The ratio of the resulting variance in flux to the surface brightness is the luminosity-weighted mean luminosity of the stars that make up the galaxy (Tonry & Schneider 1988). Because this property of the stellar population in the I band is well correlated with the $V-I$ color of the galaxy (Tonry et al. 1997), these fluctuations can be used as a high-precision distance indicator. Measurement of SBF in *Hubble Space Telescope* (*HST*) images minimizes the effects of contaminating sources of variance and are therefore ideal for SBF distance measurement. The *HST* archive provides the data necessary for the measurement of SBF in 15 galaxies in the Virgo Cluster. These observations form the data set used in this study.

Section 2 of this paper outlines the structure of the Virgo Cluster as understood from the projected distribution of members, observations of the X-ray gas, and lower precision measurements of distances to members. Section 3 describes the data set, its reduction, and the particulars of how we measured SBF in this study. (For a more general discussion of the SBF method, see Jacoby et al. 1992.) Section 4 presents the results. This section includes a comparison of the resulting distances with those found in other studies and examines the data for signs of miscalibration. Section 5 explores the implications of observations for the structures of the NGC 4486 and NGC 4472 clouds. Section 6 concludes with some final thoughts.

2. THE PROJECTED STRUCTURE OF THE VIRGO STRUCTURE

The Virgo Cluster of galaxies has an extended, complex morphology. Traditionally, its structure has been studied by dividing it up into clouds, beginning with de Vaucouleurs (1961), who separated it into groups centered on NGC 4486 and NGC 4472, which he designated groups A and B. Tanaka (1985), using velocity data to reduce contamination from background galaxies, produced a similar division of the cluster. He assigned the labels I and II to subclusters centered roughly on NGC 4486 and NGC 4472, corresponding to the A and B clouds of de Vaucouleurs (1961). X-ray data (Böhringer et al. 1994) support the identification of these two clouds as the primary structures of the Virgo Cluster. The largest concentration of hot gas, as traced by X-ray emission, is centered on NGC 4486. NGC 4472 is the center of a second, smaller concentration. This study also finds a concentration of X-ray gas around NGC 4406, suggesting that this galaxy, too, is the center of a group of galaxies. Because of the small projected distance between NGC 4406 and NGC 4486, such a group would be difficult to distinguish from the main NGC 4486 group using projected positions.

However, projected positions and velocities do show additional structure. These include the W, W′ (de Vaucouleurs 1961) and M (Ftaclas, Struble, & Fanelli 1984) clouds. Gavazzi et al. (1999) performed a more elaborate subdivision using not only spatial and velocity information, but also fundamental plane (FP) and Tully-Fisher distance measurements. The uncertainty in the distances measured using these techniques is large compared with the size of the Virgo Cluster, and the authors focus on measuring the mean distances to subsamples of galaxies. Figure 1 shows the division of the cluster as performed by Gavazzi et al. (1999). The Gavazzi et al. (1999) E, A, and N clouds correspond the A cloud of de Vaucouleurs (1961); their B cloud contains portions of the B and W′ clouds of de Vaucouleurs (1961) (though, confusingly, not NGC 4472, the central bright galaxy of the de Vaucouleurs 1961 B cloud); and their S cloud contains much of the de Vaucouleurs (1961) B cloud, including NGC 4472. The M and W clouds are similar under each system. To avoid confusion in further discussion, the de Vaucouleurs (1961) A and B clouds will be referred to as the NGC 4486 and NGC 4472 clouds, respectively.

The presence of these subclusters, particularly those centered on NGC 4486 and NGC 4472, appears fairly robust. Many different studies, using different means of isolating Virgo Cluster members from background galaxies, find similar sets of clouds. (For example, de Vaucouleurs 1961 uses only the brightest galaxies, Tanaka 1985 separates Virgo galaxies from background galaxies using radial velocities, Binggeli, Tammann, & Sandage 1987 use a subjective classification based on morphology, and Gavazzi et al. 1999 use a combination of radial velocities and distance measured using the Tully-Fisher and FP relations.)

A variety of techniques have been employed in measuring the mass of the Virgo Cluster. Recent examples include the estimate of Hoffman, Olson, & Salpeter (1980) using dynamical models of galaxies in or near the Virgo Cluster, the estimates of Tully & Shaya (1984) using virial analysis of Virgo galaxies and the infall of galaxies surrounding the Virgo Cluster, and the estimate of Böhringer et al. (1994)

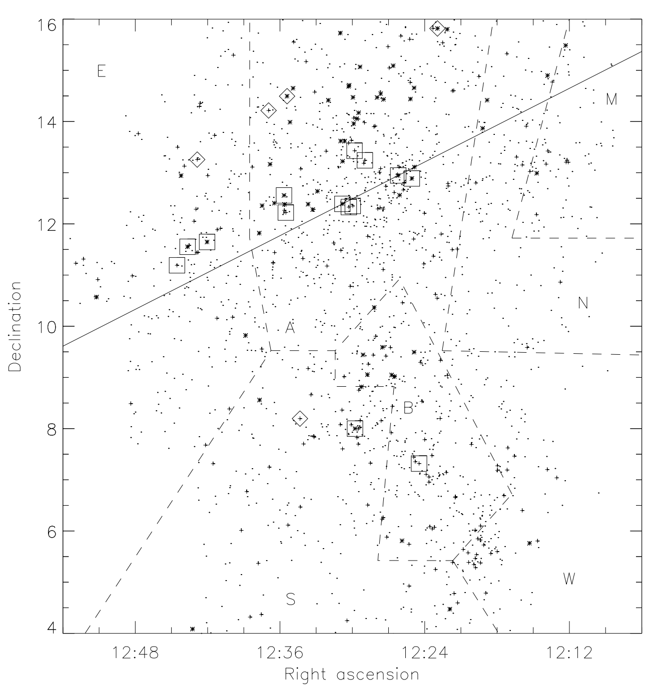

FIG. 1.—Positions of Virgo Cluster galaxies, together with the cloud boundaries as described by Gavazzi et al. (1999). The dashed lines show the boundaries between clouds, the asterisks show galaxies from the Messier catalog, the plus signs show galaxies from the NGC catalog, and the dots are galaxies from the Virgo Cluster Catalog (VCC; Binggeli, Sandage, & Tammann 1985). Galaxies with SBF distance measurements in this study are marked with boxes, and those with Cepheid distances from Ferrarese et al. (1999) are marked with diamonds. The *x*-axis of Fig. 6 is marked with a solid line.

using properties of the X-ray gas. All of these studies find masses in the range of $\sim(1\text{–}8) \times 10^{14}\, M_{\odot}$ for the NGC 4486 cloud and agree with each other to within their reported uncertainties.

3. OBSERVATIONS, REDUCTION, AND ANALYSIS

3.1. *The Sample*

Because of the exceptionally high resolution and stable point-spread function (PSF), the *HST* is an excellent instrument for the measurement of SBF. The *HST* archive contains many images of elliptical galaxies taken with the Wide Field Planetary Camera 2 (WFPC2) camera through the F814W filter (central wavelength 7921 Å, width 1489 Å). These images are ideal for the measurement of SBF because fluctuation magnitudes are relatively bright in the near infrared. This filter is close to the *I* filter, which is typically used in SBF observations from telescopes on the ground.

An indicator of the stellar populations is necessary in order to estimate the absolute magnitude of the near-IR fluctuations and thus derive a distance. Theoretical studies (Worthey 1994) and ground-based observations (Tonry et al. 1997) have shown that the $V-I$ color is a reasonable calibrator. Therefore, the archive must provide an image through a filter that can be used to estimate the V-band surface brightness of the galaxy, such as the F606W (central wavelength 5935 Å, width 1479 Å) or F555W (central wavelength 5398 Å, width 1226 Å) filters. In most cases, study of the nucleus was the original purpose of the images. One data set (that of NGC 4478) was taken as a parallel observation. In all data sets except NGC 4478, the galaxy lies in the high-resolution PC chip. NGC 4478 fell in the WF2 chip.

Table 1 lists the galaxies in the sample together with their Hubble type, magnitude, and recession velocity, as well the combined exposure times of the images used. The positions of these galaxies are shown in Figure 1.

3.2. *Initial Reduction of HST Data*

The raw data were calibrated using the WFPC2 pipeline procedure. The steps in reduction include bad pixel masking, bias and dark subtraction, and flat-field correction. The alignment of different exposures was checked using the centroids of small (usually unresolved) objects in the field, generally globular clusters. The different exposures were then combined using the CRREJ task in the STSDAS[1] package for IRAF.[2] This program removes cosmic rays by eliminating pixels that are much higher than the corresponding pixels in the other images, and the result is a higher signal-to-noise ratio image with very few cosmic rays.

3.3. *Sky Estimation*

To properly model the galaxy and measure its color in these images, it is necessary to know the sky background in the images in each filter. Ideally, one would simply measure the flux from the sky far from the galaxy. In most of these images, however, the galaxy extends well beyond the edges. Therefore, some other method is required.

[1] The Space Telescope Data Analysis System (STSDAS) is distributed by the Space Telescope Science Institute.

[2] The Image Reduction and Analysis Facility (IRAF) is distributed by the National Optical Astronomy Observatories, which are operated by the Association of Universities for Research in Astronomy (AURA), Inc., under cooperative agreement with the National Science Foundation.

TABLE 1

GALAXY AND OBSERVATION PARAMETERS

NAME	GALAXY Type	GALAXY m	V (km s^{-1})	EXPOSURE TIME F555W	EXPOSURE TIME F814W
NGC 4472 (M49)......	E2	9.37	868 ± 8[a]	1800	1800
NGC 4486 (M87)......	E0	9.59	1282 ± 9[a]	2400	2400
NGC 4649 (M60)......	E2	9.81	1413 ± 10[b]	2100	1800
NGC 4406 (M86)......	E3	9.83	−227 ± 8[a]	1500	1500
NGC 4374 (M84)......	S0	10.09	1000 ± 8[a]	1200[c]	520
NGC 4365	E3	10.52	1240 ± 12[a]	1300	1400
NGC 4621 (M59)......	E5	10.57	424 ± 12[b]	1050	1050
NGC 4552 (M89)......	E0	10.73	321 ± 12[b]	2400	1500
NGC 4473	E5	11.16	2240 ± 9[a]	1800	2000
NGC 4660	E6	12.12	1097 ± 13[a]	1000	850
NGC 4478	E2	12.36	1381 ± 13[d]	5600[e]	5600
NGC 4550	SB0	12.56	381 ± 9[a]	1200	1200
NGC 4458	E0-1	12.93	668 ± 15[a]	1200	1040
NGC 4476	SA(r)0-	13.01	1978 ± 12[d]	1500	1800
NGC 4486B...........	cE0	14.36	1486 ± 53[b]	1800	2000

[a] De Vaucouleurs et al. 1991.
[b] Binggeli et al. 1985.
[c] F547M.
[d] Simien & Prugniel 1997.
[e] F606W.

One method is to use the WFPC2 exposure time calculator, which reports the number of counts from the zodiacal light present in the observation. Scattered sunlight is not considered, so the estimate given may be off by up to 40%.

An alternate method is to fit the profile of the galaxy to a theoretical profile plus a constant background, the value of which will be the value of the sky. The major problem with this method is that the true profiles do not necessarily fit our analytical models. In this data set, fits to different ranges of radii or to different functions (exponential or de Vaucouleurs) resulted in very different estimates of the sky, often far more than 40% from the WFPC2 exposure time calculator, and sometimes even negative. Therefore, we use the estimate from the exposure time calculator in cases where the galaxy extends well beyond the edges of the image.

3.4. *SBF Measurement*

Measurement of the SBF magnitude followed the general procedure described in Tonry & Schneider (1988) and Jacoby et al. (1992). The steps taken to perform the measurement are the following:

1. Identify and mask as many contaminating objects (globular clusters, background galaxies, foreground stars, dust patches, remaining cosmic rays, etc.) as possible.
2. Model the galaxy, using modified elliptical isophotes or other methods. Subtract the model from the data image and divide the result by the square root of the model. This results in an image with uniform noise, because the most important sources of noise (photon statistics and SBF) are proportional to the square root of the signal. At this point, it may be possible to detect more contaminating objects, so an improved mask may be made. The mask and model creation steps may be iterated a few times for best results.
3. Add regions where the sky signal exceeds the galaxy signal to the mask. Inclusion of these regions will only add noise to our result.
4. Calculate $P(\mu, \nu)$, the power spectrum of the PSF, and $I(\mu, \nu)$, the power spectrum of the masked, galaxy-subtracted, noise-normalized image.
5. Fit the power spectrum of the masked, galaxy-subtracted, noise-normalized image to linear function of the PSF power spectrum: $I(\mu, \nu) = a + pP(\mu, \nu)$.
6. Correct p for the masked pixels to arrive at $\bar{f}$, the number of counts from a luminosity-weighted average luminosity star: $\bar{f} = p/(1 - m)$, where m is the fraction of pixels masked and $\bar{f}$ is the flux from our fictitious "SBF star," our standard candle.
7. Convert $\bar{f}$ to a magnitude as appropriate for the observations.
8. Estimate the effect of unmasked contaminating objects on the measurement by adding artificial populations of contaminating objects and repeating the measurement. In this data set, the error introduced by contaminating objects is less than 0.01 mag, and no correction is made.

For a detailed description of the software and procedures used to execute the measurements made in this study, see Neilsen (1999).

3.5. *Measurement of V − I Color*

To use the measured SBF magnitude as a distance indicator, the absolute magnitude of the fluctuations must be estimated. This magnitude is a function of the stellar populations present. The simplest indicator of these populations is the color, and based on models and ground-based studies the $V-I$ color and the I SBF magnitude seem to be closely correlated.

The use of the *HST* F555W and F814W filters rather than the standard V and I filters complicates both comparison with other observations and the use of ground-based calibrations. Because there are insufficient data for a more direct calibration of the *HST* filters, distances are measured using conversions from the *HST* filters to the standard V and I filters.

The simplest of these conversions is that of the color. Experiments with population models indicate that the conversions for stars determined by Holtzman et al. (1995) work reasonably well for the integrated light of galaxies as well. An equation for the *HST* $V_{\rm F555W} - I_{\rm F814W}$ color in terms of the standard $V-I$ color can be derived algebraically from the equations given in Holtzman et al. (1995). This relation is nearly linear. To determine the inverse, we calculate a grid of $V_{\rm F555W} - I_{\rm F814W}$, $V-I$ pairs and fit a second-order polynomial this set of points.

The models of Worthey (1998, private communication) include both $V-I$ and $V_{\rm F555W} - I_{\rm F814W}$ colors for a variety of stellar populations. A comparison of the $V-I$ color that would be estimated from $V_{\rm F555W} - I_{\rm F814W}$ and the conversions of Holtzman et al. (1995) with the "true" $V-I$ color of the artificial population suggests that the errors introduced by this conversion are usually small compared with other sources of error in the color measurement, such as uncertainty in the sky background.

We use the fit models of the regions of the galaxies used to measure the SBF to measure the color used to calibrate the SBF. Rather than measuring the integrated color in these regions, the color of each pixel is measured separately, and these pixel colors are averaged. This prevents the brightest regions of the galaxy from dominating the color. This is important, because the brighter regions of the galaxy do not dominate the galaxy in our SBF measurement procedure.

Direct comparison of our color measurements (reported in Table 2) with those found is ground-based studies is complicated by the color gradients found in the sample. One set that may be suitable for comparison is that of Poulin & Nieto (1994), who measure the colors of a large set of early-type galaxies in several apertures per galaxy. Their data set contains eight of the galaxies from this study: NGC 4458, 4473, 4478, 4486B, 4486, 4550, 4621, and 4660. Based on the uncertainties reported in Poulin & Nieto (1994) and estimated in this study, the weighted mean difference in color between the colors presented here and those of Poulin & Nieto (1994) is -0.04 ± 0.02, in the sense that our colors are slightly bluer at the 2 σ level. There are several reasons one might expect our colors to be bluer. First, the regions masked because they are unsuitable for SBF, such as dust and the centers of galaxies where the model fitting sometimes fails, are disproportionately red. More importantly, the aperture photometry performed in Poulin & Nieto (1994) measures the color of the combined flux within the aperture, while this study uses the mean pixel color, as described above. The bright central regions, which have a redder color the fainter outer regions, are therefore given more weight in the color measurements presented in Poulin & Nieto (1994) than those presented here, resulting in a their measuring a slightly redder color. The offset between the Poulin & Nieto (1994) colors and those presented here is therefore reasonable, although the uncertainty in the difference is such that even asserting that it is detected may not be warranted.

A more appropriate set of color measurements for comparison is that reported by Ajhar et al. (1997), who measure SBF in an *HST* archive data set that partially overlaps that of this study. Because the regions chosen are those suitable for SBF in the same archive images, a comparison between the colors determined here and those reported by Ajhar et al. (1997) will apply to similar regions of the galaxies in question. Because Ajhar et al. (1997) corrected their calibration to force the surface photometry they measure to match the surface photometry of Tonry et al. (1997), the colors Ajhar et al. (1997) report will match that of Tonry et al. (1997). A comparison between the colors measured here (which are calibrated independent of previous galaxy photometry) and those of Tonry et al. (1997) (calibrated to match the of previous galaxy photometry) is therefore meaningful. For the seven galaxies for which the samples overlap (NGC 4472, 4649, 4406, 4621, 4552, 4473, and 4660), the mean difference between the Ajhar et al. (1997) colors and those of this study is 0.09 ± 0.09. The difference was never larger then the expected uncertainty (as reported in Table 2), and usually much smaller.

3.6. *Derivation of* $\overline{M}_{I,\rm F814W}$ *versus* $V-I$ *color*

A simple conversion of the measured $\overline{m}_{I,\rm F814W}$ magnitude to an $\overline{m}_I$ magnitude using the equations of Holtzman et al.

TABLE 2

SBF Measurements and the Resultant Distances for Galaxies in Our Sample (in Mpc)

Name	$(V-I)_{\rm H}$	$m_{I,\rm F814W}$	Distance Modulus	SBF (Mpc)
NGC 4472 (M49)......	1.291 ± 0.008	29.99 ± 0.02	30.94 ± 0.09	15.4 ± 0.6
NGC 4486 (M87)......	1.263 ± 0.025	30.07 ± 0.03	31.15 ± 0.12	17.0 ± 1.0
NGC 4649 (M60)......	1.315 ± 0.009	30.21 ± 0.07	31.06 ± 0.11	16.3 ± 0.8
NGC 4406 (M86)......	1.203 ± 0.025	30.10 ± 0.03	31.45 ± 0.12	19.5 ± 1.1
NGC 4374 (M84)......	1.247 ± 0.015	30.02 ± 0.01	31.17 ± 0.10	17.1 ± 0.8
NGC 4365	1.266 ± 0.018	30.87 ± 0.11	31.94 ± 0.15	24.4 ± 1.7
NGC 4621 (M59)......	1.258 ± 0.015	29.72 ± 0.04	30.82 ± 0.10	14.6 ± 0.7
NGC 4552 (M89)......	1.266 ± 0.011	29.93 ± 0.05	31.00 ± 0.10	15.8 ± 0.7
NGC 4473	1.231 ± 0.018	29.85 ± 0.03	31.07 ± 0.11	16.4 ± 0.8
NGC 4660	1.238 ± 0.029	30.11 ± 0.09	31.30 ± 0.16	18.2 ± 1.3
NGC 4478	1.180 ± 0.017	31.08 ± 0.05	31.10 ± 0.11	16.4 ± 0.9
NGC 4550	1.173 ± 0.050	29.34 ± 0.10	30.82 ± 0.22	14.6 ± 1.5
NGC 4458	1.137 ± 0.16	30.15 ± 0.19	31.78 ± 0.59	22.7 ± 6.2
NGC 4476	1.054 ± 0.040	29.61 ± 0.04	31.60 ± 0.16	20.9 ± 1.6
NGC 4486B...........	1.197 ± 0.033	29.77 ± 0.08	31.14 ± 0.16	16.9 ± 1.3

Note.—The reported uncertainties include uncertainties in the measurement and in the Tonry et al. 1997 SBF magnitude vs. color relation, but not the uncertainty introduced by the conversion of this relation from I and V to the magnitudes measured using the F555W and F814W filters.

(1995) is unsuitable for several reasons. First, the colors of the stars that dominate the SBF are much redder than the colors for which the equations are derived. Second, it is not the color of the galaxy that one needs to use to convert the magnitudes, but the color of the SBF stars, which is more difficult to measure. Finally, not only the magnitudes vary between the filters, but the weights as well. Even if the Holtzman et al. (1995) equations were valid, and appropriate colors could be accurately measured, what one could derive using them would be the magnitude corresponding to the luminosity

$$\bar{l} = \frac{\sum_i n_i \times l_{I,\mathrm{F814}W} \times l_I}{\sum_i n_i \times l_{I,\mathrm{F814}W}}\,,$$

and not

$$\bar{l} = \frac{\sum_i n_i \times l_I^2}{\sum_i n_i \times l_I}$$

as we desire.

A better approach is to derive a relation between $\overline{m}_{I,\mathrm{F814}W}$ and some measurable property, in this study the $V-I$ color as derived from the $V_{\mathrm{F555W}} - I_{\mathrm{F814W}}$ in the images.

Ajhar et al. (1997) determined such a calibration empirically using SBF measurements from a sample of galaxies that overlaps those of this study, and distances to their sample measured using ground-based measurements of $\overline{m}_I$ and the $\overline{m}_I$ versus $V-I$ calibration of Tonry et al. (1997). Their study showed only a poor correlation between $V-I$ and $\overline{M}_I$; even after the removal of a particularly deviant measurement (NGC 4621) and assuming a "cosmic scatter" in $\overline{M}_{I,\mathrm{F814}W}$ of 0.05 mag, the χ_ν^2 of their linear fit is 1.60. This is surprising given the tight correlation ($\chi_\nu^2 = 1.10$) between $V-I$ and $\overline{m}_I$ found in Tonry et al. (1997). The Ajhar et al. (1997) results also disagree with the models of Worthey (1998, private communication), which is again surprising given how well these models agree with the calibration of Tonry et al. (1997). The triple-dot–dashed line in Figure 2 shows the Ajhar et al. (1997) calibration.

A second approach is to use these stellar population models to derive the desired relation. Hopefully, the same models that agree well with the I-band calibration should be useful for deriving the relation for F814W. The simplest way of using the models is as a method of converting the Tonry et al. (1997) relation for use with the F814W filter. For each model, the model values of $\overline{M}_I$, $\overline{M}_{I,\mathrm{F814W}}$, $V-I$, and $V_{\mathrm{F555W}} - I_{\mathrm{F814W}}$ are provided, and from these the $\overline{M}_I$ estimation of Tonry et al. (1997) from $V-I$ and the Holtzman et al. (1995) estimation of $V-I$ from $(V-I)_{\mathrm{Holtzman}}$ ($\equiv V_{\mathrm{F555W}} - I_{\mathrm{F814W}}$) can be calculated. We can now estimate the conversion of the Tonry et al. (1997) calibration to a relationship between $\overline{M}_{I,\mathrm{F814W}}$ and $(V-I)_{\mathrm{Holtzman}}$ by fitting $\overline{M}_{I,\mathrm{empirical}} + (\overline{M}_{I,\mathrm{F814W}} - \overline{M}_I)$ to $(V-I)_{\mathrm{Holtzman}}$, shown in dot-dashed line of Figure 2.

Which models are the most appropriate for use in this conversion is uncertain. Many of the models fall far from the empirical calibration line of Tonry et al. (1997), and may not be appropriate for actual galaxies. Furthermore, few galaxies are likely to consist of single populations. Therefore, we created a set of combination models, which provide model information for galaxies consisting of two populations, one younger and more metal-rich than the other, in various proportions. The subset of these models which lie close to the empirical calibration of Tonry et al. (1997) are then used for further model-based calibrations of the $\overline{M}_{I,\mathrm{F814W}}, (V-I)_{\mathrm{Holtzman}}$ relation.

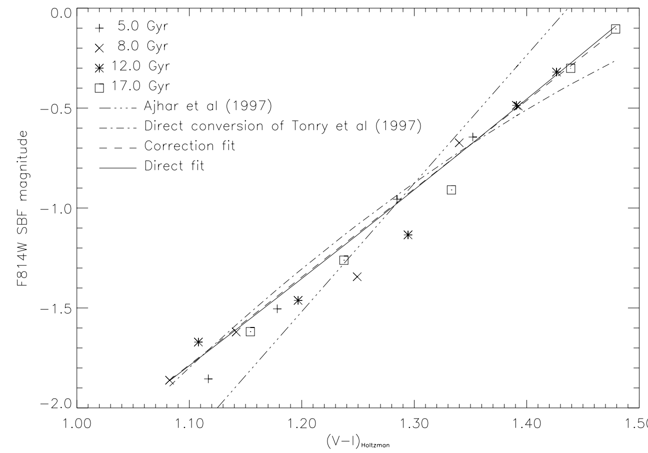

FIG. 2.—Conversion of the I-band calibration to an F814W calibration using the Worthey models. The plus signs, crosses, asterisks, and squares represent models with ages of 5, 8, 12, and 17 Gyr, respectively. The triple-dot–dashed line represents the Ajhar et al. (1997) calibration, The dot-dashed line represents the Tonry et al. (1997) I-band calibration converted to F814W using a fit to the models. The dashed line represents the model using a correction fit only to mixtures of populations for which the model is a good fit. Last, the solid line is a direct fit to such population mixtures.

One of these is to use these models as we used the single population models, fitting $\overline{M}_{I,\mathrm{empirical}} + (\overline{M}_{I,\mathrm{F814W}} - \overline{M}_I)$ to $(V-I)_{\mathrm{Holtzman}}$, shown as the dashed line in Figure 2. Finally, $\overline{M}_{I,\mathrm{F814W}}$ can be fitted to $(V-I)_{\mathrm{Holtzman}}$ directly, shown as the solid line. Because the models were chosen to be those that agreed well with the I-band empirical calibration, this last fit is probably the most realistic of the calibrations discussed, and is used as the calibration for the remainder of this study. This calibration is

$$\overline{M}_{I,\mathrm{F814W}} = -5.98 + 3.31(V-I)_{\mathrm{Holtzman}} + 0.46(V-I)^2_{\mathrm{Holtzman}}\,.$$

The second-order fit is used not to improve the precision of the calibration (the difference between the first- and second-order fits is much smaller than the expected uncertainty in the calibration), but rather to ensure that this calibration is as close as possible to the Tonry et al. (1997) calibration for purposes of comparison.

It is important to note that all of the calibration models derived using the Worthey (1998, private communication) models agree well with each other, and even adopting the calibration of Ajhar et al. (1997) is unlikely to significantly affect the relative positions of most of the galaxies. Most galaxies in the sample fall in a narrow range of colors ($V-I \simeq 1.26 \pm 0.04$); distance moduli for these galaxies will be systematically closer if the Ajhar et al. (1997) calibrations are used, but small scatter in color for these galaxies minimizes the effect of the calibration difference on the relative positions measured. The positions of the bluest galaxies in the sample (also the faintest) relative to the rest of the sample are more sensitive to the differences in calibration. Adopting the Ajhar et al. (1997) calibration would place these blue galaxies further than they would appear with the other calibrations.

4. RESULTS

4.1. *SBF Distances to Virgo Galaxies*

Table 2 displays the $V-I$ colors of the regions used for SBF, as determined by a conversion of the measured $m_{V,\mathrm{F555W}} - m_{I,\mathrm{F814W}}$ to $V-I$ using the empirical relation of Holtzman et al. (1995), the measured SBF magnitude $\overline{m}_{I,\mathrm{F814W}}$, the distance modulus resulting from this measurement and the converted SBF calibration of Tonry et al. (1997), and the corresponding distance. The error estimates in the distance and distance modulus include uncertainties in the background subtraction and statistics, uncertainty in the calibration of Tonry et al. (1997), and the uncertainty in the calibration due to uncertainty in the measured color, but do not include uncertainty in the photometric zero points and conversions, conversion of the SBF calibration, or reddening.

4.2. *Comparison with other Distance Measurements*

Figure 3 shows the distribution of the differences between distance moduli measured in this study and those measured in other studies using SBF and other methods. The top left panel shows the difference with the ground-based SBF measurements. A variety of papers provided measured values of $\overline{m}_I$ and $V-I$ (Tonry, Ajhar, & Luppino 1990, Ciardullo, Jacoby, & Tonry 1993, Ajhar et al. 1997), and distance measurements were determined using the calibration of Tonry et al. (1997). While the distance moduli are in agreement for most of the sample, NGC 4660 and NGC 4458 show discrepant values. The exposure times for these galaxies are among the shortest in our sample, and the uncertainties in the resultant distance moduli are among the largest. However, at least in the case of NGC 4660, the expected uncertainty is not large enough to accommodate a difference of 0.8 mag. The remaining galaxies are in good agreement. The mean difference is very close to 0.0, and the scatter in the differences is close to that expected from the estimated uncertainties. This is a good indication that errors introduced by the conversion of the Tonry et al. (1997) I-band calibration to the F814W filter are modest compared with other sources of uncertainty.

The second-to-top row in Figure 3 shows the difference between our results and the SBF measurements of Ajhar et al. (1997) using the same *HST* data, but with the method and software applied to the ground-based data described above. NGC 4660 and NGC 4458 are again in strong dis-

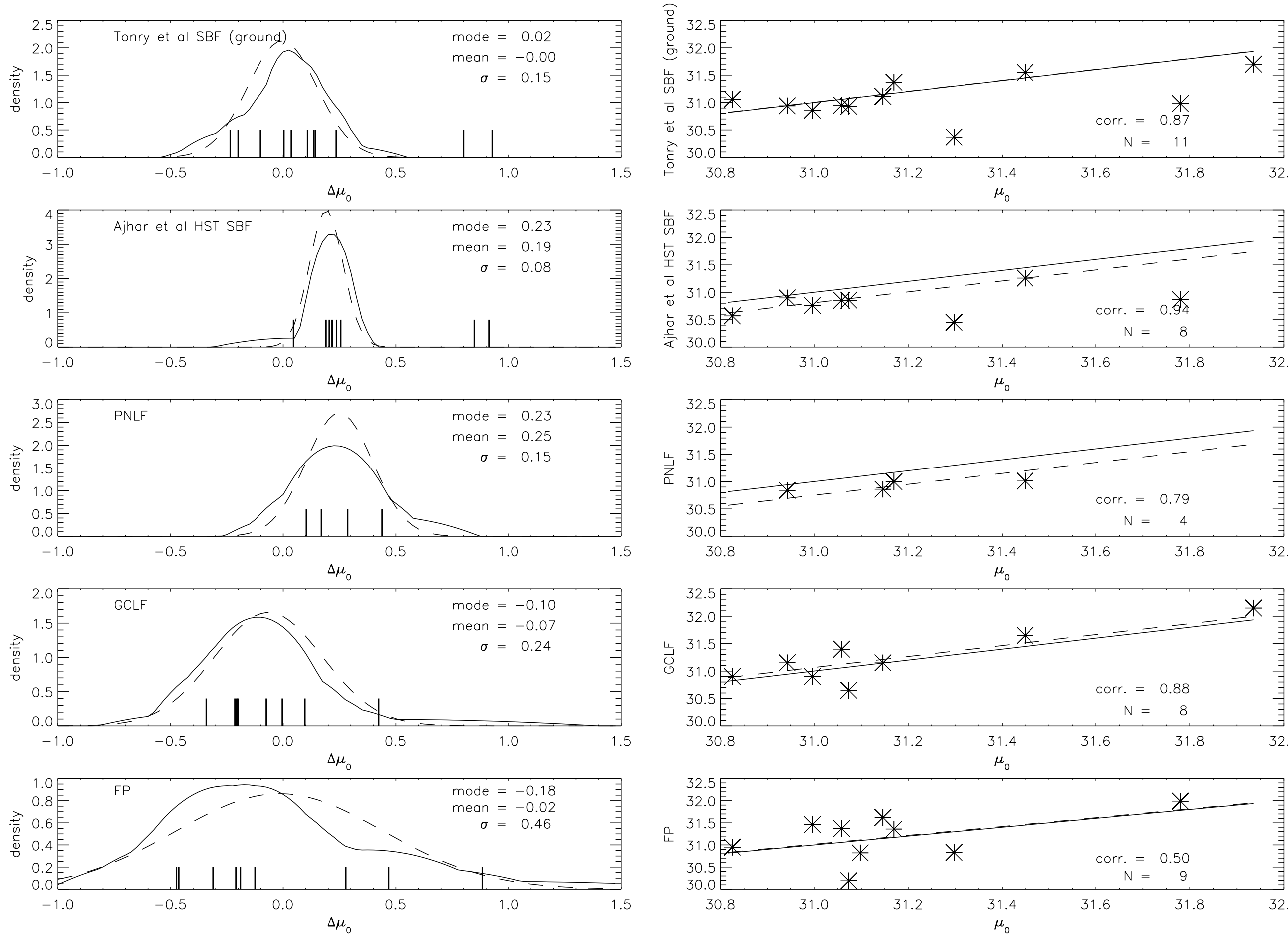

FIG. 3.—Each plot compares the SBF distance moduli presented here with those found in other studies. *Left*: Distribution of the differences between the different distance moduli for the same galaxy. Positive values indicate that this study found a greater distance modulus. The ticks along the bottom of each plot indicate the values for individual galaxies, the solid line is a variable width Epanechnikov kernel smoothing of these points, and the dashed line is a Gaussian matching the mean and width of the points, sometimes excluding the most discrepant measurements. *Right*: Distance modulus in the other study as a function of the distance modulus in this study. The solid line represents a perfect match.

agreement, indicating the difference lies in the reduction of the data and measurement of SBFs, rather than in a difference in the data. NGC 4472 also lies apart from the main cluster of data points. Its separation is due entirely to the correction for undetected globular clusters. Ajhar et al. (1997) apply a correction of 0.1 mag to compensate for undetected globular clusters. After experiments with simulated data sets and the addition of artificial clusters to the data images, no such correction was found to be necessary in our study. If identical corrections for NGC 4472 are applied to both measurements, or if NGC 4472 is removed from the comparison sample, the scatter in the differences drops to $\sigma = 0.03$ mag (again excluding NGC 4660 and NGC 4458). Differences in background estimates, regions chosen for SBF, and other procedural differences can account for such a scatter. Slightly more surprising is the offset of 0.19 mag (0.22, if NGC 4472 is not considered). This offset is due to an offset in the calibrations. As discussed in § 4, we use a theoretical conversion of the empirical calibration of Tonry et al. (1997), while Ajhar et al. (1997) use a fit of $\overline{M}_{I,\mathrm{F814W}}$, as determined from their measurements and ground -based SBF distance moduli, to their measured $V-I$ colors. The reduced χ^2 of the Ajhar et al. (1997) calibration indicates a poor fit, and identification and removal of outliers can result in significantly different calibrations (for example, see Ferrarese et al. 1999). As indicated in § 4, the different calibrations result in an offset between the distances, but little difference in relative positions.

The middle row in Figure 3 shows the comparison with the distance moduli derived from the turnover of the planetary nebula luminosity function (PNLF), as reported in Ciardullo et al. (1993). This method, first suggested by Hodge (1966) and implemented by Ford & Jenner (1978), uses the bright end of the PNLF as a standard candle. The scatter of the differences between the PNLF distance moduli and the SBF distances presented here is $\sigma = 0.15$, consistent with that expected from the reported uncertainties, even if uncertainties in the SBF calibration are neglected. There is a 0.25 mag offset between the SBF results presented here and the PNLF measurements. This is disturbing, but in agreement with other comparisons. Ferrarese et al. (1999) find that, at the distance of Virgo and greater, PNLF distances are significantly shorter than those derived from SBF, and that the discrepancy worsens at greater distances. Error in SBF due to incomplete masks, resulting in contamination by globular clusters and background galaxies, would increase with distance. However, such errors would cause the measured distance to be underestimated, which only increases the disagreement with the PNLF distances. Mendez (1999) suggests that there may be significant contamination of the PNLF by intracluster planetary nebulae, and that such a contamination may cause the distance modulus to be underestimated by up to 0.2 mag. Work by Ciardullo et al. (1998) supports this proposal. Such a difference could bring the PNLF and SBF results presented here into agreement.

The second-to-bottom row in Figure 3 shows the difference between the SBF distance moduli and the distance measured from the peak of the globular cluster luminosity function (GCLF), using the same data set (Neilsen 1999). In this plot, the absolute magnitude of the peak is assumed to be roughly that of the Milky Way and M31, $M_{0,V} = -7.4$ Ashman & Zepf (1998). Agreement between the SBF distance moduli and those from the GCLF are consistent with the expected uncertainties. The dispersion in the differences is consistent with the expected uncertainty in the measurement in the peak of the GCLF.

The bottom row in Figure 3 shows the difference between the SBF distance moduli and the distance measured using the FP relation for early-type galaxies as measured in Gavazzi et al. (1999). The FP relation uses known correlations between the velocity dispersion and surface brightness with the luminosity and radius of an early-type galaxy to use the galaxy itself as a standard candle (or ruler). The mean difference between the FP distances reported in Gavazzi et al. (1999) and the SBF distances reported here is close to zero, and the scatter with $\sigma = 0.46$, which is very close to the uncertainty of 0.45 for the FP distance moduli, as determined from the scatter in the FP relation. Neither the NGC 4458 nor the NGC 4660 distances were more than 1 σ away from agreement in this comparison and were not excluded in the comparison as they were in the comparisons with Ajhar et al. (1997) and Tonry et al. (1997). Unfortunately, the uncertainty in the FP distance measurements are too large to play a significant role in resolving the discrepancies in the distances to NGC 4458 and NGC 4660.

4.3. *Calibration Accuracy*

If the calibration used to produce the SBF distances has been chosen correctly, then there should be no significant correlation between the distance modulus measured and the color of the galaxy. Figure 4 (*top*) shows the distance modulus of each galaxy against the color of that galaxy. The

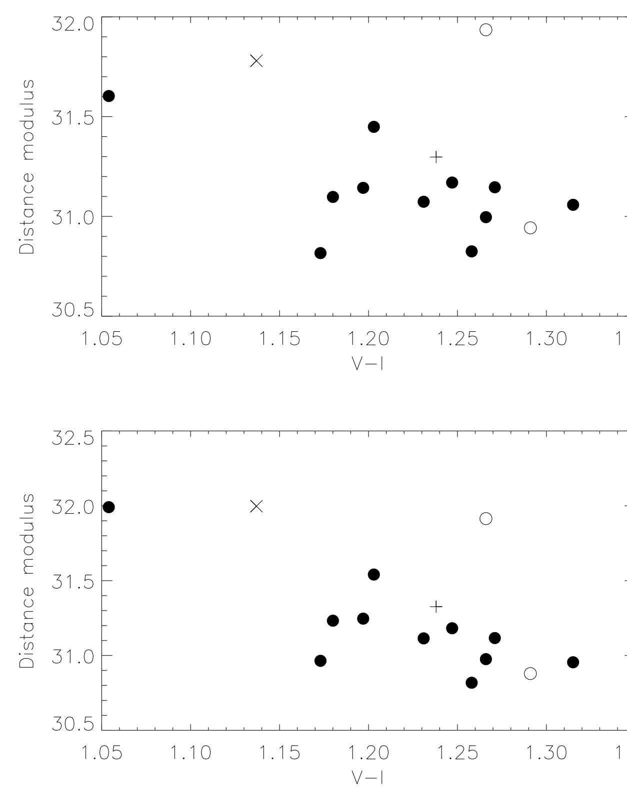

FIG. 4.—Points show the measured distance modulus as a function of the $V-I$ color of the observed galaxy. The open circles represent NGC 4472 and NGC 4365, which are not members of the NGC 4486 cloud. The crosses mark NGC 4458, which has a much higher uncertainty than any other data point, and the plus signs mark NGC 4660, which may be corrupted by unmasked dust. The top plot shows the results using the calibration used in this study, while the bottom plot shows the results calibrated using Ajhar et al. (1997).

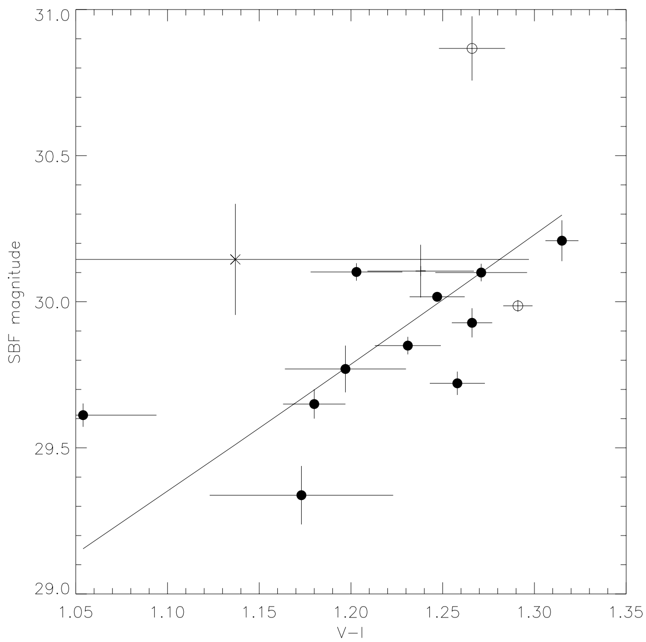

FIG. 5.—Measured SBF magnitude as a function of color. The open data points represent NGC 4472 and NGC 4365, which are not members of the NGC 4486 cloud. The crosses mark NGC 4458, which has a much higher uncertainty than any other data point, and the plus signs mark NGC 4660, which may be corrupted by unmasked dust. The line shows the relation between color and magnitude assumed by the calibration used in this study.

correlation coefficient between the color and distance modulus is -0.39, which is not statistically significant for the sample size of 15. The distances to most of the galaxies are consistent with the distance to NGC 4486, with a few galaxies appearing either in front or behind the NGC 4486 cloud. If these data are calibrated using the relation of Ajhar et al. (1997), in Figure 4 (*bottom*), the resulting correlation coefficient is -0.64, which is significant with 98% confidence.

Figure 5 shows the measured SBF magnitude as a function of measured $V-I$ color. The line shows the estimated relation between absolute SBF magnitude and galaxy color. If all galaxies were at the same distance and our calibration were correct, all data points would lie along this line. Although most data points lie along this line, several do not. This indicates that most galaxies have the same distance, while a few lie in the foreground or background. If instead of using our calibration, we fit a line (including the errors in both color and SBF magnitude), the best-fit line fits poorly: the reduced χ^2 of the best-fit line to the NGC 4486 cloud galaxies rejects the fit with better than 99.9% confidence. Because the best-fit line minimizes the reduced χ^2, all other lines can be rejected with greater confidence. Therefore, the presence of galaxies with a distance significantly different than that of the center of the cloud cannot be an effect of miscalibration.

5. DISCUSSION

5.1. *The NGC 4486 Cloud*

Table 1 and Table 2 present the parameters of the galaxies in this sample. The last two galaxies listed (NGC 4472 and NGC 4365) are members of the NGC 4472 cloud, while the remainder appear in the NGC 4486 cloud. As can be seen from Figure 1, the projected positions of the sample galaxies lie near a line passing through NGC 4406 and NGC 4486, shown by the solid line in that figure. This alignment arises partially from the elongation of the NGC 4486 cloud in this direction, and partially because the *HST* archive contained few observations of galaxies far from this line.

To study the spatial arrangement of the sample, we first transform the known positions and measured distances into a rectangular coordinate system centered on NGC 4486, where the z-axis is the line from Earth to NGC 4486 and increases with increasing distance; the x-axis lies along the line from NGC 4486 to NGC 4406 (Fig. 1, *solid line*), where NGC 4406 is in the $+x$ direction from NGC 4486; the y is such that we have a standard Cartesian coordinate system. The galaxies in the NGC 4486 cloud with SBF distances all have y coordinates close to 0, so the positions can be effectively plotted in the (x, z) plane. Figure 6 shows the positions of these galaxies on the (x, z) plane. Two features are apparent from the plot: first, there is much greater elongation in the z direction than in the x direction, and second, many of the galaxies do lie close to NGC 4486. These qualities suggest that there is a central concentration of galaxies near NGC 4486, with outliers in the foreground and background.

All of the sample galaxies in the NGC 4486 cloud fall either into the Gavazzi et al. (1999) A or E clouds. Those with $x < -0.5$ in Figure 6 are in the E cloud. The others lie in the A cloud. The general distribution of distances appears similar in the E and A clouds.

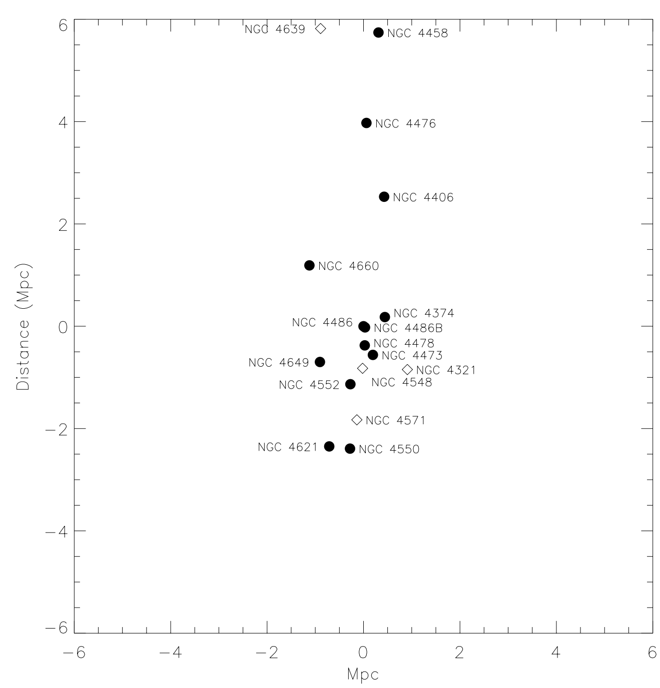

FIG. 6.—Depth map of the NGC 4486 cloud of the Virgo Cluster. Galaxies are plotted on the x-z plane described in the text. The abscissa lies along the line plotted in Fig. 1 and corresponds to the x-axis described in the text. The ordinate lies along the line of sight (into the paper in Fig. 1), corresponding to the z-axis described in the text. The filled circles represent galaxies with SBF distance estimates from this study, and the diamonds represent galaxies with Cepheid distances from Ferrarese et al. (1999).

The galaxies with Cepheid distance from Ferrarese et al. (1999), shown as diamonds in Figure 6, are generally similar to the SBF distances measured. NGC 4639 appears to be in the background of the E cloud. NGC 4571 and NGC 4548 appear in the midst of the SBF galaxies near NGC 4486 and follow the trend of increasing distance with increasing x. Even though it is located at significantly greater x, the distance to NGC 4321 is similar to that of galaxies near NGC 4486.

The SBF distance moduli of NGC 4486 cloud galaxies, which fall between 30.82 and 31.45, are in generally good agreement with the Gavazzi et al. (1999) distance moduli of 30.84 ± 0.06 and 31.23 ± 0.16 for their A and E clouds. (We note here that the Gavazzi et al. 1999 distances were measured using the FP and Tully-Fisher techniques, which have uncertainties for individual galaxies of approximately 0.45 and 0.35 mag, respectively. The small errors on the Gavazzi et al. 1999 distance moduli for the different clouds are the result of measuring a sample of galaxies in each cloud.)

An examination of heliocentric velocity as a function of position can provide some information on the dynamics of the cluster as well. Figure 7 shows the relation between distance and velocity for our sample. The line shows the velocity expected from a Hubble expansion assuming $H_0 = 75$ km s^{-1} Mpc^{-1}. NGC 4458 is plotted twice, showing the contradicting velocity values found in the literature. A number of galaxies have velocities far from those expected from the Hubble expansion, suggesting some sort of complex dynamics. Three of the four nearest galaxies all have velocities much lower than expected, suggesting that they have been accelerated away from the Virgo Cluster and toward the Local Group. NGC 4406 also has a much lower velocity than expected and lies behind the majority of our sample; it is falling in from behind. NGC 4473 is the only galaxy with a velocity that is significantly larger than expected. As the distance measured places it near the center of the NGC 4486 cloud, this suggests that it has fallen into the cluster from the front. It is also clear that two galaxies that were apparently associated with the NGC 4486 cloud, NGC 4476 and NGC 4458, really lie in the background.

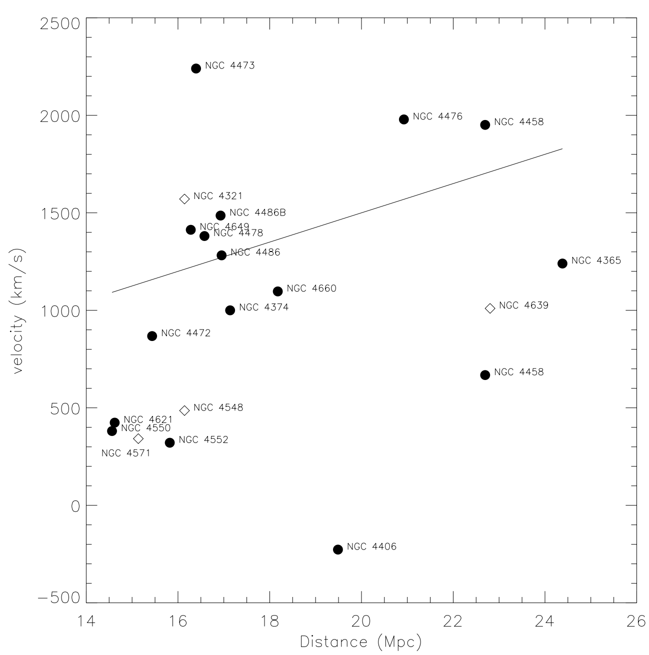

FIG. 7.—Distance as a function of heliocentric velocity. The two points shown for NGC 4458 show the two discrepant velocities found in the literature. The solid line shows the expected expansion velocity (when $H_0 = 75$) corresponding to the given distance. The filled circles represent galaxies with SBF distances from this study, and the open diamonds represent galaxies with Cepheid distances from Ferrarese et al. (1999).

With both distances and radial velocities for our sample, we examine the dynamics of the NGC 4486 cloud using a simple model. If we take (based on the X-ray data of Böhringer et al. 1994) NGC 4486 to be the center of the NGC 4486 cloud, we can get the distance between each galaxy and the center of this cloud. If we make the simplistic assumption that each galaxy is moving either directly toward or away from this center, a total velocity can be estimated. Because our sample in this cloud is significantly elongated along the line of sight, the resulting total velocities will be very close to the difference in heliocentric velocities between NGC 4486 and each galaxy. Once distances and velocities have been estimated, we can derive the total mass the cloud must have in order for each galaxy to be gravitationally bound. The mass at which the galaxy becomes bound is that at which its total energy is zero,

$$\frac{1}{2}mv^2 - \frac{GMm}{r} = 0 ,$$

and therefore,

$$M = \frac{rv^2}{2G} .$$

Figure 8 shows this minimum mass as a function of distance from NGC 4486. Several things are apparent from this plot. If we compare these minimum masses with the X-ray based mass estimates of Nulsen & Böhringer (1995) and Böhringer et al. (1994), most galaxies appear to be bound. These galaxies also appear bound when the minimum masses are compared with mass estimates based on dynamical models, which agree well with the X-ray estimates (as discussed in § 2). Particularly at large distances, minimum binding masses for most galaxies are within an order of magnitude of the estimated mass for Virgo's NGC 4486 cloud.

Although the precision of the measurement for each galaxy is still to low to draw any definite conclusions, there are several interesting cases that invite speculation. First, NGC 4406 appears at best only barely gravitationally bound. Gravitational attraction to the NGC 4486 cloud is probably only part of the explanation for its unusual blueshift. Three galaxies, NGC 4621, NGC 4550, and NGC 4552, appear to be (borderline) gravitationally bound despite moving away from NGC 4486 with a large velocity. Because they are only a few megaparsecs away from NGC 4486, this velocity cannot be entirely explained by the Hubble expansion. NGC 4621, for example, is moving away from NGC 4486 with a velocity of 858 km s^{-1}, only 180 km s^{-1} of which is attributable to the Hubble flow. One plausible explanation is that these galaxies began on the far side of NGC 4486, accelerated toward it, and have emerged on the near side. To examine the timescales over which this could occur, let us consider a simple model. If one neglects interactions and rotation, and assumes the estimated NGC 4486 cloud mass of $\sim 4 \times 10^{14}\, M_{\odot}$ to be uniformly distributed (more concentrated distributions result in shorter

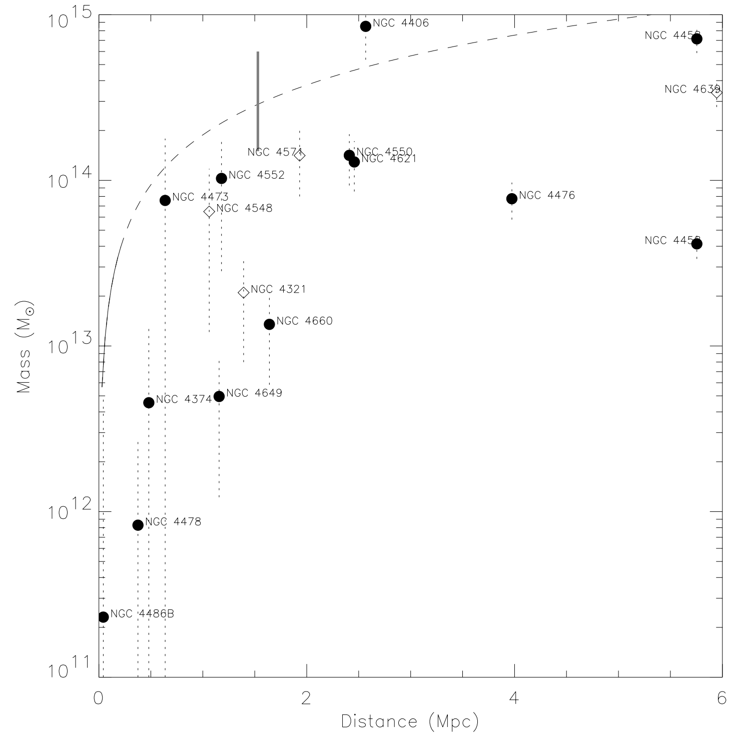

FIG. 8.—Minimum mass of the NGC 4486 cloud of the Virgo Cluster for each galaxy to be gravitationally bound. The plotted error bars include distance and velocity error uncertainties. Note that the galaxies at smaller distances have much larger error bars because the uncertainty in the distance is large in comparison with the measured distance. The solid line shows a model based on X-ray data from Nulsen & Böhringer (1995). The dashed line shows the extrapolation of this model beyond the X-ray data on which it is based. The thick vertical line shows the mass estimate from Böhringer et al. (1994). The filled circles represent galaxies with SBF distances from this study, and the open diamonds represent galaxies with Cepheid distances from Ferrarese et al. (1999).

timescales) within the inner few megaparsecs of the cluster, the motion of a galaxy through it can be described as a simple harmonic oscillator. In this highly simplified model, it would take NGC 4621, for example, 10 Gyr to fall from the far side of NGC 4486 to its current position. Larger masses for the Virgo Cluster and more concentrated mass distributions result in shorter times. Therefore, the universe appears to be old enough to accommodate this model. In any case, given the close proximity to NGC 4486 and low heliocentric velocities compared with the Hubble flow, it seems plausible that these galaxies were behind NGC 4486 sometime in the history of the universe.

5.2. *The NGC 4472 Cloud*

There are too few members of the NGC 4472 cloud in our sample to give a good indication of its position relative to the NGC 4486 cloud. Our measurements of NGC 4472 itself indicate that it lies at a distance similar to that of NGC 4486, perhaps slightly nearer. The Cepheid distance to NGC 4535 (Ferrarese et al. 1999), also in the NGC 4472 cloud (and S cloud of Gavazzi et al. 1999) is consistent with this SBF distance to NGC 4472. The NGC 4472 SBF distance modulus of 30.94 is in good agreement with the Gavazzi et al. (1999) distance modulus 30.91 ± 0.10 for the S cloud.

NGC 4365, located in the W′ cloud of de Vaucouleurs (1961) and the B cloud of Gavazzi et al. (1999), is much further than NGC 4472 and most of the galaxies in the NGC 4486 cloud. Its distance modulus of 31.94 is in good agreement with the Gavazzi et al. (1999) distance modulus 31.84 ± 0.10 for the B cloud.

6. CONCLUSION

For most galaxies where there is overlap, the *HST* SBF distances presented here are in good agreement with other distance measurement methods. Based on these results, the NGC 4486 cloud of the Virgo Cluster appears to be significantly elongated along the line of sight, perhaps showing an increase in distance along the elongation axis running from NGC 4486 to NGC 4406. Simple models indicate that the NGC 4486 cloud is probably gravitationally bound (though not necessarily at statistical equilibrium) and that some of the galaxies currently on the near side of NGC 4486 probably began behind it.

This sample contains too few galaxies in other clouds of the Virgo Cluster to allow further examination. However, the distances found by this study confirm the distances to these clouds as determined by other distance measurement methods, particularly the Cepheid distances compiled in Ferrarese et al. (1999) and the FP and Tully-Fisher distances presented in Gavazzi et al. (1999).

We are grateful to Guy Worthey for providing us with data for his stellar population models in the *HST* filter set, to Laura Ferrarese for providing us with Cepheid distances to Virgo Cluster galaxies measured as part of the *HST* Key Project, and to Holland Ford, Brad Whitmore, Francois Schweizer, and Rosemary Wyse for useful advice, criticism, and discussion. We also thank the referee, John Tonry, for valuable suggestions that improved this paper. Support for this work was provided by NASA through grant GO-7543 from the Space Telescope Science Institute, which is operated by AURA, Inc., under NASA contract NAS 5-26555.

REFERENCES

Ajhar, E. A., Lauer, T. R., Tonry, J. L., Blakeslee, J. P., Dressler, A., Holtzman, J. A., & Postman, M. 1997, AJ, 114, 626
Ashman, K. M., & Zepf, S. E. 1998, Globular Cluster Systems (Cambridge: Cambridge Univ. Press)
Binggeli, B., Sandage, A., & Tammann, G. A. 1985, AJ, 90, 1681
Binggeli, B., Tammann, G. A., & Sandage, A. 1987, AJ, 94, 251
Böhringer, H., Briel, U. G., Schwarz, R. A., Voges, W., Hartner, G., & Trumper, J. 1994, Nature, 368, 828
Ciardullo, R., Jacoby, G. H., Feldmeier, J. J., & Bartlett, R. E. 1998, ApJ, 492, 62
Ciardullo, R., Jacoby, G. H., & Tonry, J. L. 1993, ApJ, 419, 479
de Vaucouleurs, G. 1961, ApJS, 6, 213
de Vaucouleurs, G., de Vaucouleurs, A., Corwin, H. G., Jr., Buta, R. J., Paturel, G., & Fouqué, P. 1991, Third Reference Catalogue of Bright Galaxies (New York: Springer)
Ferrarese, L., et al. 2000, ApJ, 529, 745
Ford, H. C., & Jenner, D. C. 1978, BAAS, 10, 665
Ftaclas, C., Struble, M. F., & Fanelli, M. N. 1984, ApJ, 282, 19
Gavazzi, G., Boselli, A., Scodeggio, M., Pierini, D., & Belsole, E. 1999, MNRAS, 304, 595
Hodge, P. W. 1966, The Physics and Astronomy of Galaxies and Cosmology (New York: McGraw-Hill)
Hoffman, G. L., Olson, D. W., & Salpeter, E. E. 1980, ApJ, 242, 861
Holtzman, J. A., Burrows, C. J., Casertano, S., Hester, J. J., Trauger, J. T., Watson, A. M., & Worthey, G. 1995, PASP, 107, 1065
Jacoby, G. H., et al. 1992, PASP, 104, 599
Mendez, R. H. 1999, in Post-*Hipparcos* Cosmic Candles, ed. A. Heck & F. Caputo (Dordrecht: Kluwer), 161
Neilsen, E. H., Jr. 1999, Ph.D. thesis, Johns Hopkins Univ.
Nulsen, P. E. J., & Böhringer, H. 1995, MNRAS, 274, 1093
Poulin, P., & Nieto, J. 1994, A&AS, 103, 573
Simien, F., & Prugniel, P. 1997, A&AS, 122, 521
Tanaka, K. I. 1985, PASJ, 37, 427
Tonry, J. L., Ajhar, E. A., & Luppino, G. A. 1990, AJ, 100, 1416
Tonry, J. L., Blakeslee, J. P., Ajhar, E. A., & Dressler, A. 1997, ApJ, 475, 399
Tonry, J., & Schneider, D. P. 1988, AJ, 96, 807
Tully, R. B., & Shaya, E. J. 1984, ApJ, 281, 31
Worthey, G. 1994, ApJS, 95, 107